Nano Research
2023, 16(2): 3287–3293

ISSN 1998-0124 CN 11-5974/O4
https://doi.org/10.1007/s12274-022-4915-0

Research Article

Th-MOF showing six-fold imide-sealed pockets for middle-size-separation of propane from natural gas

Li Wang[1], Wenhui Zhang[1], Jie Ding[1], Lele Gong[1], Rajamani Krishna[2], Youyuan Ran[1], Lan Chen[1], and Feng Luo[1] (✉)

[1] *Jiangxi Province Key Laboratory of Synthetic Chemistry, School of Chemistry, Biology and Material Science, East China University of Technology, Nanchang 330013, China*

[2] *Van't Hoff Institute for Molecular Sciences, University of Amsterdam, Science Park 904, 1098 XH Amsterdam, The Netherlands*

Received: 17 June 2022 / **Revised:** 30 July 2022 / **Accepted:** 16 August 2022

ABSTRACT

Separation of propane from natural gas is of great importance to industry. However, in light of size-based separation, there still lacks effective method to directly separate propane from natural gas, due to the comparable physical properties for these light alkanes (C1–C4) and the middle size of propane. In this work, we found that a new Th-metal-organic framework (MOF) could be an ideal solution for this issue. The Th-MOF takes UiO-66-type structure, but with the pocket sealed by six-fold imide groups; this not only precisely reduces the size of pocket to exactly match propane, but also enhances the host–guest interactions through multiple (C)H($^{\delta+}$)···($^{\delta-}$)O(C) interactions. As a result, highly selective adsorption of propane over methane, ethane, and butane was observed, implying unique middle-size separation. The actual separation was confirmed by breakthrough experiments of simulated natural gas, confirming its superior application in direct separation of propane from natural gas. The separation mechanism, as unveiled by both theoretical calculation and comparative experiments, is due to the six-fold imide-sealed pocket that could effectively distinguish propane from other light alkanes through both size effect and host–guest interactions.

KEYWORDS

Th-metal-organic framework (MOF), intermediate-size-separation, natural gas, selectivity

1 Instructions

Natural gas (NG) widely exists on the earth, with abundant reserves, such as oilfield gas, gas field gas, mud volcanic gas, coalbed methane, and biogenic gas. It contains both light hydrocarbon and nonhydrocarbon gases. The major component of light hydrocarbon consists of methane (85%), ethane (9%), propane (3%), and butane (1%) [1–7]. Light alkanes play important roles in commodity production in the fuels and chemical industry. For instance, CH_4 is used as clean fuel, C_2H_6 is the used as raw materials for different reactions such as the manufacture of polymer, and propane is an important raw material for modern industry [8–10]. In China, the propane consumption in 2019 was 16.57 million tons [11]. Therefore, separation of these hydrocarbons is a prerequisite for effective utilization of these resources.

The kinetic diameter of methane, ethane, propane, and butane is 3.8, 4.4, 4.3–5.1, and 4.7 Å, respectively, implying difficult separation of this mixture, due to the comparable size [12–15]. But they exhibit different molecule sizes such as 3.76 Å × 3.83 Å × 3.99 Å for methane, 4.08 Å × 4.29 Å × 4.72 Å for ethane, 4.02 Å × 4.79 Å × 6.20 Å for propane, and 4.02 Å × 4.61 Å × 7.38 Å for butane. This suggested that we can separate this mixture through precisely designing pore structure and size. Due to the outstanding importance of propane in the industry, there demands urgent concern about direct generation of propane from natural gas (mainly quaternary gas mixture of methane, ethane, propane, and butane) [16–19]. However, to enforce this target, there still lacks available metal-organic frameworks (MOFs) or effective molecular design strategy to match exactly the size of propane. On the other hand, in light of size-based separation that is often designed and employed for separation in the field of MOFs, both the kinetic diameter and the molecular size of propane are located at the middle among these mixtures, implying a demand of middle-size separation [20]. However, this is seriously restricted for common molecular design and most available MOFs. To the best of our knowledge, there is still no report about direct separation of propane from natural gas until this work.

The size and configuration of pore in MOFs present a highly important factor for separation [21–26]. MOFs could selectively adsorb gas molecules with smaller size than the pore of MOFs, but will exclude these gas molecules with bigger size than the pore of MOFs [27, 28]. And co-adsorption would occur when all the components in the gas mixture have smaller size than the pore of MOFs; this often leads to weak or no separation [29–31]. Thereby, separation of molecules with middle size among the gas mixture remains a challenging task [32, 33]. Flexible framework with gate opening could be a good resolution. For example, just the target molecule with middle size can result in the gate opening, and other molecules with relatively smaller size or bigger size could not result in the gate opening, consequently leading to selective adsorption of middle-size molecules. This unique phenomenon has been realized by Zhang et al. for separation of styrene from the ethylbenzene/styrene/toluene/benzene mixture [20]. However, this type of separation is highly dependent on the magnitude of

Address correspondence to ecitluofeng@163.com

host–guest interactions, thus restricting its application for other mixtures.

Anchoring functionalized units on the pore wall of MOFs to enhance the host–guest interactions is also an effective method for separation [34–36]. This can theoretically selectively adsorb target molecule from the mixture under precise design on the functionalized units. However, this method could be also invalid to perform middle-size separation for these molecules with similar structure and physical properties.

In this work, we found that the combination of size control and anchoring functionalized units is an effective solution to give middle-size separation for propane from natural gas (see Scheme 1). The used MOF shows the pore size bigger than methane, ethane, and propane, but less than butane, and the pore wall is decorated by three-fold imide groups that act as strong H-acceptor to enhance host–guest interactions. Selective adsorption of propane over methane and ethane is due to the relatively stronger host–guest interactions between propane and MOFs, while selective adsorption of propane over butane is due to the big size of butane (relative to the pore of MOF).

2 Experimental

Caution! $Th(NO_3)_4$ used in this study is radioactive and chemically toxic reactant, so standard precautions and protection for handling such substances were followed. Other chemicals are directly purchased from Innochem without further purification.

2.1 Synthesis of N,N′-bis-(4-benzoic acid)-1,4,5,8-naphthalenediimide (H_2L)

10 mmol (2.68 g) 1,4,5,8-naphthalenetetracarboxylicdianhydride (NTCDA) was weighted in a 250-mL round-bottom flask. 50 mL dried acetic acid was added and stirred for 10 min. Then 20 mmol (2.74 g) 4-aminobenzoic acid was added in the solution and allowed reflux at 119 °C. After 12 h, the reaction was cooled to room temperature. The product was washed by distilled water and ethanol through filtration and dried in vacuum.

2.2 Synthesis of ECUT-Th-10

15 mg H_2L and 8 mg $Th(NO_3)_4$ were mixed together in N,N-dimethylformamide (DMF). Then 100 μL perchloric acid was added in the mixture. The mixture was placed into screw-capped glass vial and sealed. The vial was heated at 110 °C for 72 h. After that, the system was cooled down to room temperature. The light orange crystals (**ECUT-Th-10**) were obtained after washing by DMF. The details for the experiments are shown in the Electronic Supplementary Material (ESM).

3 Results and discussion

3.1 Structure of ECUT-Th-10

The MOF, namely **ECUT-Th-10**, was synthesized by the solvothermal reaction of $Th(NO_3)_4$, N,N'-bis-(4-benzoic acid)-1,4,5,8-naphthalenediimide (H_2L), and perchloric acid. Light orange octahedral crystals were obtained (Fig. S1 in the ESM). The purity of the as-synthesized samples was confirmed by powder X-ray diffraction (PXRD) tests (Fig. S2 in the ESM). Single-crystal X-ray diffraction analysis shows that **ECUT-Th-10** crystallizes in the cubic space group *Fd-3m* with big unit cell of $a = b = c =$ 39.5857(7) Å and large volume of 62,032(3) Å^3 (Table S4 in the ESM). The asymmetric unit contains one crystallography-independent Th(IV), which is coordinated by four carboxylate oxygen atoms from four different L^{2-} ligands, two μ^3-OH ions, and two μ^3-O^{2-} ions, forming a square antiprismatic geometry (Fig. 1(b)). The Th–O bonds are in the normal range, comparable with

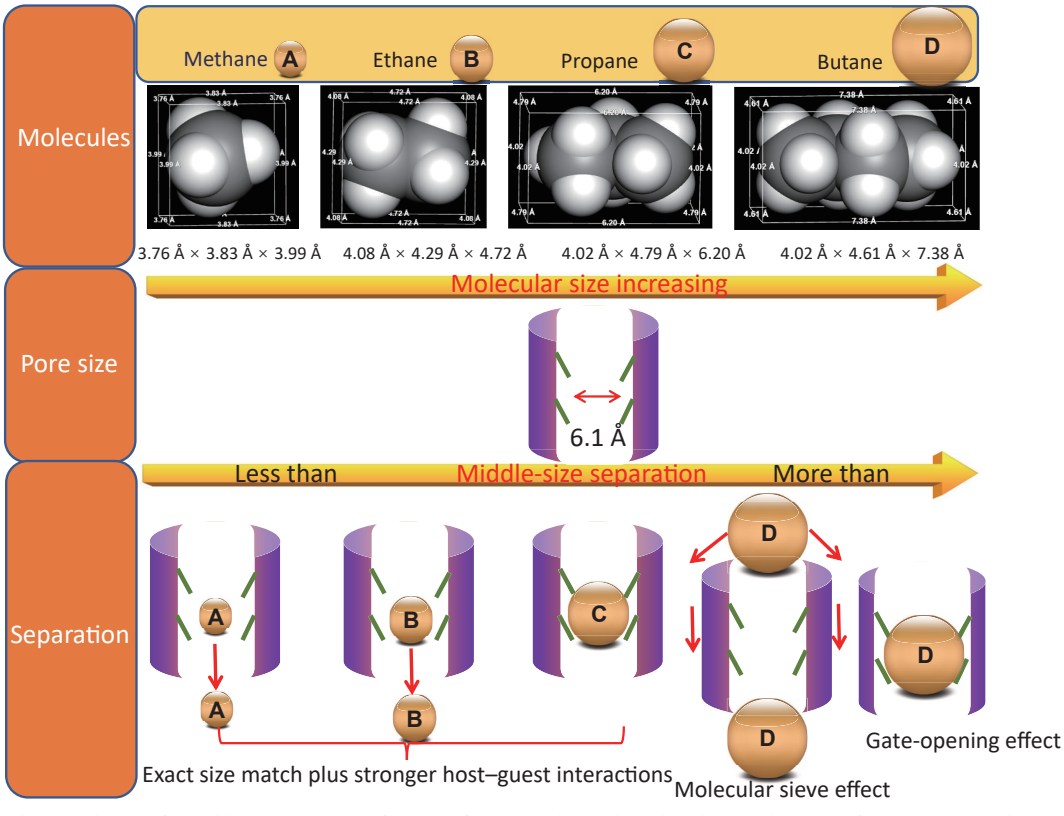

Scheme 1 The schematic diagram for middle-size separation of propane from natural gas, where the selective adsorption of propane over methane and ethane is due to the exact match of molecular size with the pore of MOF plus enhanced host–guest interactions resulted from anchoring functionalized units, while the selective adsorption of propane over butane is due to the size effect, since the molecular size of butane is bigger than the pore size. In addition, this MOF shows a gate-opening adsorption for butane as the pressure increases.

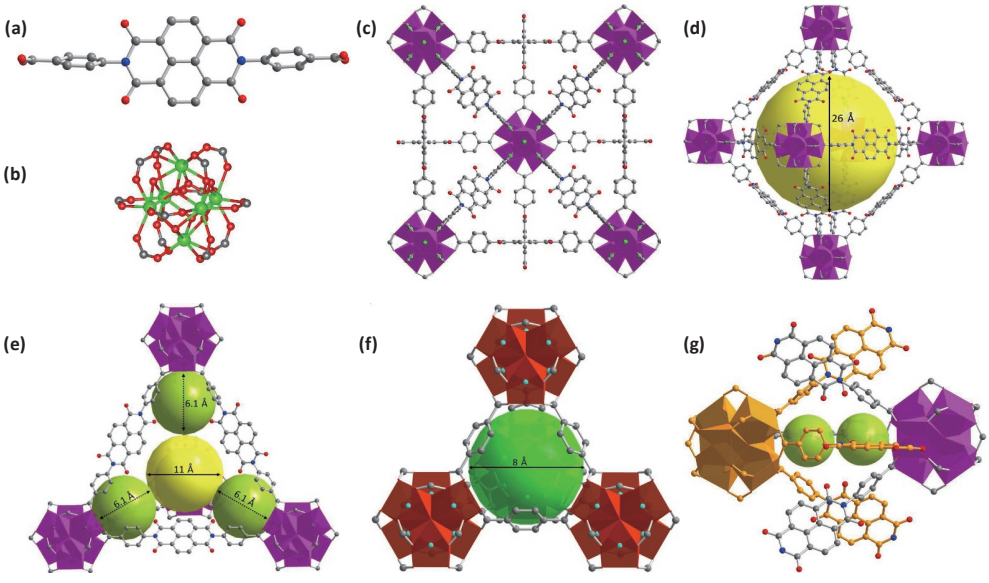

Figure 1 The structure of **ECUT-Th-10**. (a) The ligand H_2L. (b) The $Th_6(\mu^3\text{-}OH)_4(\mu^3\text{-}O^{2-})_4$ building block. (c) The UiO-66-type structure of **ECUT-Th-10**. (d) The octahedral cage in **ECUT-Th-10**. (e) The tetrahedral cage in **ECUT-Th-10** with four unique three-fold imide-sealed pockets at the vertex of tetrahedral cage. (f) A comparison of the tetrahedral cage in UiO-66. (g) The unique six-fold imide-sealed pockets formed by interpenetration. The H atoms in the framework were omitted for clarity.

that observed in the literature (Table S5 in the ESM) [37, 38]. The L^{2-} ligands afford the bidentate mode to connect to four Th(IV) ions. Due to steric hindrance, the middle imide-containing fragment is rotated and almost perpendicular to the two terminal benzene rings, as evidenced by the dihedral angle of 88.97° and 88.53° between them (Fig. 1(a)).

Through μ^3-OH ions and μ^3-O^{2-} ions, six identical Th(IV) ions are integrated to generate a $Th_6(\mu^3\text{-}OH)_4(\mu^3\text{-}O^{2-})_4$ building block, which is very similar with the well-known $Zr_6(\mu^3\text{-}OH)_4(\mu^3\text{-}O^{2-})_4$ building block in UiO-66-type structures. Each $Th_6(\mu^3\text{-}OH)_4(\mu^3\text{-}O^{2-})_4$ core connects to twelve L^{2-} ligands, and an overall UiO-66-type structure is observed in **ECUT-Th-10** (Fig. 1(c)). Interestingly, as observed in UiO-66, **ECUT-Th-10** also affords two different cages of octahedral and tetrahedral cages. However, the octahedral cage is as large as to 2.6 nm, due to the use of long ligand of L^{2-} (Fig. 1(d)). The tetrahedral cage in **ECUT-Th-10** is divided into two types of pores, and four three-fold imide-sealed pockets are observed at the vertex of tetrahedral cage that gives the aperture of 6.1 Å (Fig. 1(e)); this is impressively matchable with the size of propane, but bigger than methane and ethane, and smaller than butane, implying its potential for selective adsorption of propane over methane, ethane, and butane, finally leading to middle-size separation. However, UiO-66 just shows one type of pore for tetrahedral cage with a size of about 8 Å (Fig. 1(f)). The formation of unique three-fold imide-sealed pockets in **ECUT-Th-10** is due to the use of L^{2-} ligands that show the rotation of imide-containing fragment and result in a perpendicular configuration for the L^{2-} ligand between the middle imide-containing fragment and two terminal benzene rings, and finally cause the imide C=O bonds to orient inside the tetrahedral cage. Notably, two-fold interpenetration is observed in **ECUT-Th-10**, which largely reduces the pore. And the three-fold imide-sealed pockets are then further sealed by additional three imide units from another net, constructing the overall six-fold imide-sealed pockets (Fig. 1(g)).

3.2 Thermogravimetric analysis (TGA)

To confirm the permanent porosity, we first carried out TGA of **ECUT-Th-10**, showing that the guest molecules can be removed before 250 °C (Fig. S3 in the ESM). But this can be decreased through CH_3OH treatment, since the CH_3OH-exchanged samples showed the solvent loss before 100 °C. Therefore, the activation of **ECUT-Th-10** was prepared at 100 °C under vacuum. The TGA curve of activated **ECUT-Th-10** indicated that the guest molecules have been removed since only little weight loss was observed between 100 and 450 °C (Fig. S3 in the ESM). The similar PXRD patterns of activated **ECUT-Th-10** and synthesized **ECUT-Th-10** proved that the framework structure was well maintained in activated **ECUT-Th-10** (Fig. S2 in the ESM).

3.3 Porosity measurement

To check the porosity, N_2 adsorption-desorption behavior was studied at 77 K. As shown in Fig. 2(a), the uptake capacity of N_2 is around 250 cm^3/g at 1 bar. The Brunauer–Emmett–Teller (BET) surface area was calculated to be 854 m^2/g. The theoretical pore volume of **ECUT-Th-10** was calculated to be 0.609 cm^3/g, while the practical pore volume was 0.384 cm^3/g. The size distribution gives a narrow pore at 0.63 nm and broad pore at 1.3 nm, where the narrow pore belongs to the six-fold imide-sealed pockets and the broad pore belongs to the reduced pore (such as the pristine large octahedral cage) due to interpenetration.

3.4 Pure gas adsorption isotherms

The above results further motivate us to investigate its application in separation of natural gas. First, the single component isotherms of CH_4, C_2H_6, C_3H_8, and n-C_4H_{10} were measured at 298 K, respectively (Fig. 2(b)). The uptake at 298 K and 101 kPa is 2.89 mmol/g (C_3H_8), 2.69 mmol/g (C_4H_{10}), 1.72 mmol/g (C_2H_6), and 0.42 mmol/g (CH_4), respectively, suggesting selective adsorption of propane over methane, ethane, and butane. Especially, no adsorption for C_4H_{10} at low pressure before 13 kPa is observed, implying that butane is excluded from **ECUT-Th-10** under this condition, since the size of butane is bigger than the pore size of six-fold imide-sealed pockets. As for methane, ethane, and propane, similar phenomenon is not observed, because their sizes are smaller than the pore size of six- fold imide-sealed pockets. Thereby, the adsorption ratio at low pressure (13 kPa) is as high as to 30 for C_3H_8/C_4H_{10}, 3.75 for C_3H_8/C_2H_6, and 17.1 for C_3H_8/CH_4, strongly indicative of selective adsorption towards propane. The sharp increase after 13 kPa observed in the adsorption isotherm for butane is mainly resulted from gate opening, owning to somewhat flexibility of the MOF. Gate opening is often encountered in MOFs and is generally used for

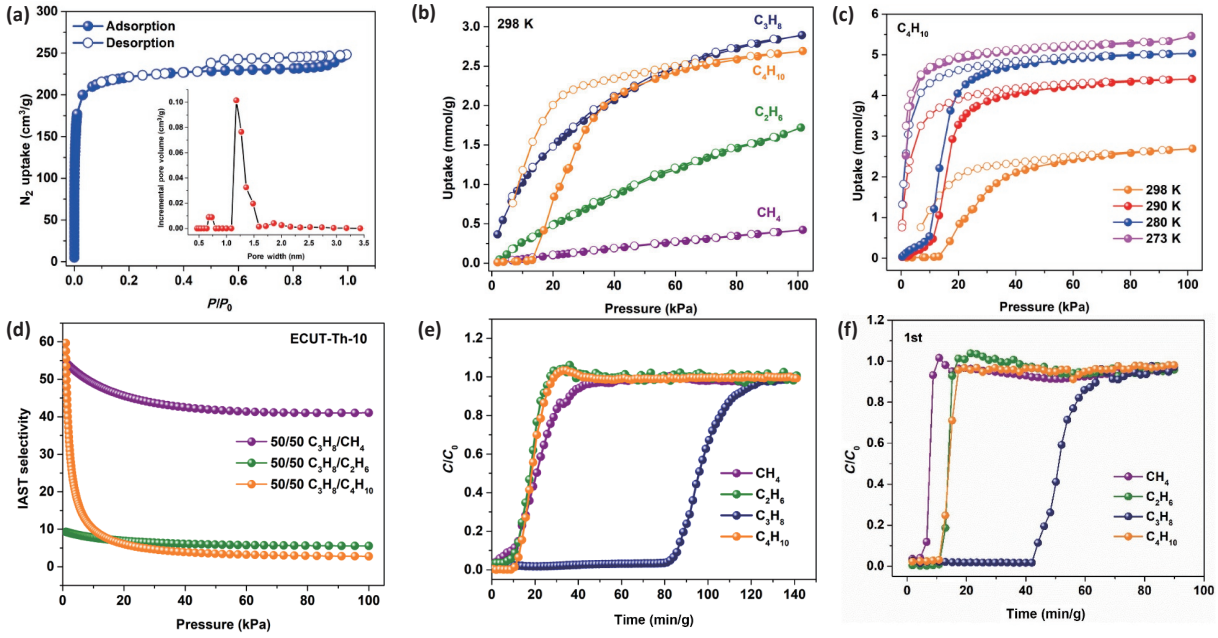

Figure 2 The adsorption and separation research upon **ECUT-Th-10**. (a) The adsorption isotherm of N_2 at 77 K with the insert of pore size distribution. (b) The adsorption isotherms of CH_4, C_2H_6, C_3H_8, and C_4H_{10} at 298 K. (c) The adsorption isotherms of C_4H_{10} at different temperatures. (d) The IAST selectivity for C_3H_8/CH_4 (50/50), C_3H_8/C_2H_6 (50/50), and C_3H_8/C_4H_{10} (50/50) in **ECUT-Th-10**. (e) Experimental breakthrough curves for $CH_4/C_2H_6/C_3H_8/C_4H_{10}$ (25/25/25/25, v/v/v/v) 4-component mixture at 298 K. (f) Experimental breakthrough curves for simulated natural gas (methane 85%, ethane 9%, propane 3%, nitrogen 2%, *n*-butane 1%) at 298 K.

separation [39–41]. The gate opening for butane is further confirmed by other adsorption isotherms at various temperatures (290 and 280 K, Fig. 2(c)). Since we used the same batch of **ECUT-Th-10** to obtain the adsorption isotherms at 290 and 280 K, it can be inferred that the framework structure still be flexible when butane was desorbed. The adsorption isotherms for C_4H_{10} at various temperatures indicated that the gate-opening phenomenon disappeared gradually as temperature decreased.

The adsorption selectivity was also evaluated by ideal adsorption solution theory (IAST), in light of the above single component isotherms at 298 K (Fig. 2(d)) [42–44]. Ultrahigh selectivity up to 60 for C_3H_8/C_4H_{10} (50:50 v/v), 9.31 for C_3H_8/C_2H_6 (50:50 v/v), and 54.5 for C_3H_8/CH_4 (50:50 v/v) is respectively observed at the onset of adsorption, also suggesting selective adsorption of propane.

We further investigated the host–guest interaction between **ECUT-Th-10** and these gases, which is mainly reflected on the isosteric heat of adsorption (Q_{st}). Thus, the adsorption of these gases at 273 K was carried out (Fig. S4 in the ESM). Due to the gate opening in C_4H_{10}, its fitting of the adsorption isotherms at 298 K cannot obtain a reasonable value, thus its Q_{st} value cannot be estimated. The Q_{st} value for other gases gives the hierarchy of C_3H_8 (33.6 kJ/mol) > C_2H_6 (27.3 kJ/mol) > CH_4 (26.4 kJ/mol), implying stronger host–guest interactions for propane (Fig. S5 in the ESM).

3.5 Breakthrough experiments

To evaluate the actual separation ability of **ECUT-Th-10** in natural gas, we further carried out breakthrough experiments at 298 K. Initially, we investigated the separation of equimolar C_3H_8 and C_2H_6 mixtures (50:50, v/v), as both of them hold closer molecule size and smaller size than the pore of six-fold imide-sealed pockets that means inevitable co-adsorption and consequently weak or no separation. As shown in Fig. S6 in the ESM, C_2H_6 is first eluted through the bed within 32 min/g, whereas C_3H_8 breaks through after 70 min/g, clearly showing separation of C_3H_8 from C_3H_8/C_2H_6 mixture. To confirm this, we repeated the experiments twice, and repeatable results were observed, suggesting excellent recyclability for the present MOF adsorbent (Fig. S7 in the ESM). Then, equimolar 3-component $CH_4/C_2H_6/C_3H_8$ mixture was measured, and all the components show smaller size than the pore of six-fold imide-sealed pockets (Fig. S8 in the ESM). Notably, clearly separation for C_3H_8 is also observed, as evidenced by the sequence of outgoing gas such as 10 min/g for CH_4, 20 min/g for C_2H_6, and 48 min/g for C_3H_8. Furthermore, we also measured the equimolar 3-component $C_2H_6/C_3H_8/C_4H_{10}$ mixture, where C_4H_{10} shows bigger size than the pore of six-fold imide-sealed pockets. As expected, C_3H_8 can be also completely separated from this mixture, and the retention time for C_2H_6 and C_4H_{10} is about 10 min/g and the corresponding value for C_3H_8 is as long as 42 min/g (Fig. S9 in the ESM). Finally, we carried out the breakthrough experiments with equimolar quaternary $CH_4/C_2H_6/C_3H_8/C_4H_{10}$ mixture at 298 K and the results are shown in Fig. 2(e). It is impressive that middle-size separation of C_3H_8 from this quaternary mixture is observed, and very long retention time up to 83 min/g is observed for C_3H_8, while CH_4, C_2H_6, and C_4H_{10} just render short retention time within 15 min/g, implying excellent separation of C_3H_8 from this quaternary mixture. The results suggest its superior application for direct separation of propane from natural gas.

To further prove the separation of C_3H_8 from the natural gas, the breakthrough experiments of **ECUT-Th-10** were performed using simulated natural gas including methane 85%, ethane 9%, propane 3%, nitrogen 2%, and *n*-butane 1% (Fig. 2(f)). The adsorption isotherm of N_2 was performed at 298 K (Fig. S10 in the ESM). The low uptake of N_2 for **ECUT-Th-10** indicated the existence of N_2 in natural gas will not affect the separation ability. The results of breakthrough experiments showed that C_3H_8 could be retained for 42 min/g, which is longer than CH_4 (4 min/g), C_2H_6 (11 min/g), and C_4H_{10} (11 min/g). The breakthrough experiments were repeated in triplicate, and no obvious decease was observed in the separation of C_3H_8, indicative of the good recyclability for **ECUT-Th-10** (Fig. S11 in the ESM).

To disclose the separation mechanism, we further carried out additionally comparative experiment. Due to the high similarity of

our MOF with UiO-66 in the structural aspect, in conjunction with the difference in the aspect of tetrahedral cage, UiO-66 was selected to give a comparative research. UiO-66 was synthesized by solvothermal method [45]. The purity of the as-synthesized UiO-66 was confirmed by PXRD tests (Fig. S12 in the ESM). The tetrahedral cage in UiO-66 is about 8 Å, which is bigger than the molecular size of methane, ethane, propane, and butane. Accordingly, middle-size separation is not expected for UiO-66. Then, we first tested the single component isotherms of CH_4, C_2H_6, C_3H_8, and n-C_4H_{10} at 298 K, respectively, giving the adsorption capacity in the hierarchy of n-C_4H_{10} (4.5 mmol/g) > C_3H_8 (4.0 mmol/g) > C_2H_6 (2.3 mmol/g) > CH_4 (0.5 mmol/g) (Fig. 3(a)). The results mean that the adsorption capacity of these gases increases along with increasing molecular size of gas molecules, completely excluding the selective adsorption of middle-size molecule as observed in **ECUT-Th-10**. Gate opening in UiO-66 is also not observed for butane, since it affords bigger tetrahedral cage than the molecular size of butane. Moreover, the corresponding C_3H_8/C_4H_{10}, C_3H_8/C_2H_6, and C_3H_8/CH_4 adsorption selectivity was also calculated, giving S = 0.4, 2.0, and 32 at the onset of adsorption, respectively (Fig. 3(b)). This value is fairly less than that observed in our MOF such as S = 60, 9.31, and 54.5, respectively, which is mainly due to the reduced size and enhanced host–guest interactions from the six-fold imide-sealed pockets in **ECUT-Th-10**. The adsorption ratio at 13 kPa in UiO-66 is 0.65 for C_3H_8/C_4H_{10}, 1.93 for C_3H_8/C_2H_6, 26.15 for C_3H_8/CH_4, indicative of the hard propane extraction (Fig. 3(c)). The absence of middle-size separation was further confirmed by breakthrough experiments from the equimolar quaternary $CH_4/C_2H_6/C_3H_8/C_4H_{10}$ mixture at 298 K, where the breakthrough sequence also obeys the order of molecular size (Fig. 3(d)). In light of these comparative experiment results, we can reason the mechanism of middle-size separation in **ECUT-Th-10** from the unique six-fold imide-sealed pockets that gives matchable size and enhanced host–guest interactions with propane over other gases such as methane, ethane, and butane.

3.6 Theoretical calculation

To obtain the structural information after adsorption of gas molecules, we then carried out density functional theory (DFT) calculation. It is found that the adsorption of these gas molecules is located at both six-fold imide-sealed pockets and three-fold imide-sealed pockets. The calculated binding energies between these gas molecules and three-fold imide-sealed pockets are −24.66 kJ/mol (CH_4), −36.84 kJ/mol (C_2H_6), −96.97 kJ/mol (C_3H_8), and −80.42 kJ/mol (C_4H_{10}), respectively. This means that the adsorption of CH_4, C_2H_6, C_3H_8, and C_4H_{10} is thermodynamically spontaneous, owing to their molecular size less than the pore of the three-fold imide-sealed pockets. The results also indicate preferable adsorption of C_3H_8 over other gas molecules and next preferable adsorption of C_4H_{10} over CH_4 and C_2H_6.

At the six-fold imide-sealed pocket, the binding energies are calculated to be −34.74 kJ/mol (CH_4), −48.98 kJ/mol (C_2H_6), −55.61 kJ/mol (C_3H_8), and −39.79 kJ/mol (C_4H_{10}), respectively. Notably, the adsorption of C_4H_{10} in the six-fold imide-sealed pocket will induce a sharp structural change (Fig. S13 in the ESM), due to that the size of C_4H_{10} is bigger than the pore of the six-fold imide-sealed pocket.

Thus, to accommodate C_4H_{10} in the six-fold imide-sealed pocket, gate opening will occur, consistent with the experimental results. In addition, it is found that C_3H_8 in the six-fold imide-sealed pocket is stabilized by multiple (C)H($^{\delta+}$)···($^{\delta-}$)O(C) interactions from imide units with a distance of 3.10(3)–3.55(3) Å (Fig. 4). By contrast, weak (C)H($^{\delta+}$)···($^{\delta-}$)O(C) interactions are observed for CH_4 with a distance of 4.17(3)–4.30(3) Å and C_2H_6 with a distance of 3.22(3)–3.89(3) Å (Figs. S14 and S15 in the

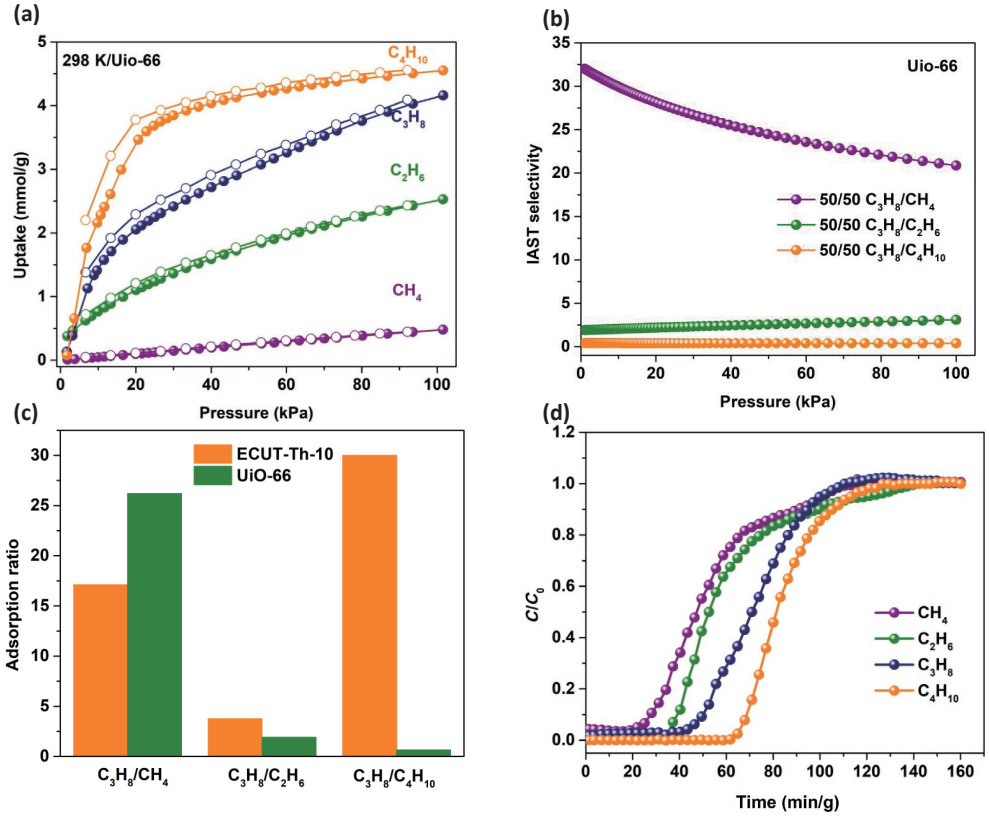

Figure 3 The adsorption and selectivity of UiO-66. (a) The adsorption isotherms of UiO-66 for CH_4, C_2H_6, C_3H_8, and C_4H_{10}. (b) The IAST selectivity data of UiO-66 for different gases. (c) The adsorption ratio for **ECUT-Th-10** and UiO-66 at 13 kPa. (d) Experimental breakthrough curves of UiO-66 for $CH_4/C_2H_6/C_3H_8/C_4H_{10}$ (25/25/25/25, v/v/v/v) 4-component mixture at 298 K.

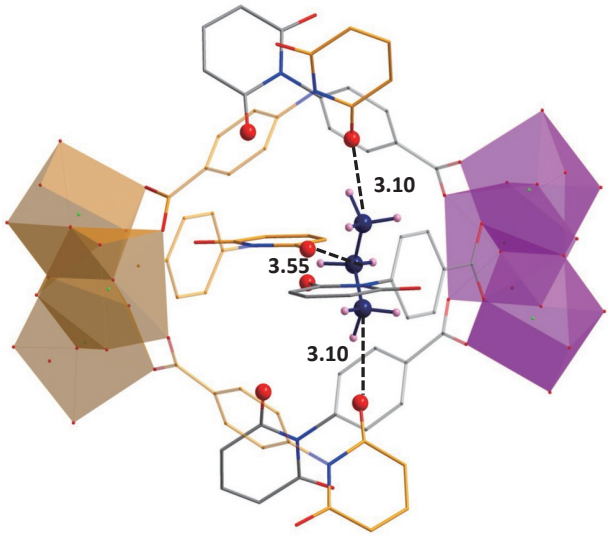

Figure 4 The (C)H($^{\delta+}$)···($^{\delta-}$)O(C) interaction between C_3H_8 and six-fold imide-sealed pockets. The H atoms in the framework were omitted for clarity.

ESM). Thereby, (C)H($^{\delta+}$)···($^{\delta-}$)O(C) interactions from the imide units enhancing the host–guest interaction for C_3H_8 are also responsible for the middle-size separation. All the results indicate that the cooperative effect between six-fold imide-sealed pockets and three-fold imide-sealed pockets is beneficial for separation of propane from natural gas.

4 Conclusions

In summary, we reported a novel MOF, **ECUT-Th-10**, which holds the UiO-66-type structure, but is constructed by diimide-based ligands and enables an interpenetrated structure with the formation of unique six-fold imide-sealed pockets. These structural merits are beneficial to separating propane from the methane/ethane/propane/butane mixture, demonstrated an extremely rare case of middle-size separation, suggesting its big potential in direct generation of propane from natural mixture. The pocket-like cage exhibits an excellent molecular sieving effect to block larger C_4H_{10}, while imide units within this pocket-like cage provide multiple (C)H($^{\delta+}$)···($^{\delta-}$)O(C) interactions with propane, thus enhancing the host–guest interactions for propane, consequently reducing the co-adsorption for methane, ethane, and propane and performing highly selective adsorption towards propane.

Acknowledgements

We thank the Open Fund of Jiangxi Province Key Laboratory of Synthetic Chemistry (No. JXSC202007), the Foundation of Jiangxi Educational Committee (No. GJJ200734), the Doctoral Scientific Research Start-up Foundation of East China University of Technology (No. DHBK2018044), the National Natural Science Foundation of China (Nos. 21966002 and 21871047), the Training Program for Academic and Technical Leaders of Major Disciplines in Jiangxi Province (No. 20194BCJ22010), the Fuzhou Youth Leading Talent Project (No. 2020ED64), and the Provincial College Students Innovation and Entrepreneurship Training Program (No. S202110405026).

Electronic Supplementary Material: Supplementary material (the details of synthesis, structural information, and other characterizations) is available in the online version of this article at https://doi.org/10.1007/s12274-022-4915-0.

References

[1] Zhang, Y. B.; Yang, L. F.; Wang, L. Y.; Cui, X. L.; Xing, H. B. Pillar iodination in functional boron cage hybrid supramolecular frameworks for high performance separation of light hydrocarbons. *J. Mater. Chem. A* **2019**, *7*, 27560–27566.

[2] Wu, Y. F.; Sun, Y. W.; Xiao, J.; Wang, X.; Li, Z. Glycine-modified HKUST-1 with simultaneously enhanced moisture stability and improved adsorption for light hydrocarbons separation. *ACS Sustainable Chem. Eng.* **2019**, *7*, 1557–1563.

[3] Wang, J.; Krishna, R.; Yang, T.; Deng, S. G. Nitrogen-rich microporous carbons for highly selective separation of light hydrocarbons. *J. Mater. Chem. A* **2016**, *4*, 13957–13966.

[4] He, Y. B.; Krishna, R.; Chen, B. L. Metal-organic frameworks with potential for energy-efficient adsorptive separation of light hydrocarbons. *Energy Environ. Sci.* **2012**, *5*, 9107–9120.

[5] Peng, Y. L.; Wang, T.; Jin, C. N.; Li, P. F.; Suepaul, S.; Beemer, G.; Chen, Y.; Krishna, R.; Cheng, P.; Pham, T. et al. A robust heterometallic ultramicroporous MOF with ultrahigh selectivity for propyne/propylene separation. *J. Mater. Chem. A* **2021**, *9*, 2850–2856.

[6] Borah, B.; Zhang, H. D.; Snurr, R. Q. Diffusion of methane and other alkanes in metal-organic frameworks for natural gas storage. *Chem. Eng. Sci.* **2015**, *124*, 135–143.

[7] Wu, Y. Q.; Weckhuysen, B. M. Separation and purification of hydrocarbons with porous materials. *Angew. Chem., Int. Ed.* **2021**, *60*, 18930–18949.

[8] Wang, Y. T.; Fan, W. D.; Wang, X.; Han, Y. F.; Zhang, L. L.; Liu, D.; Dai, F. N.; Sun, D. F. Solvent-induced framework-interpenetration isomers of Cu MOFs for efficient light hydrocarbon separation. *Inorg. Chem. Front.* **2018**, *5*, 2408–2412.

[9] Li, L.; Yin, Q.; Li, H. F.; Liu, T. F.; Cao, R. Rational design of phosphonocarboxylate metal-organic frameworks for light hydrocarbon separations. *Mater. Chem. Front.* **2018**, *2*, 1436–1440.

[10] Chen, Y. W.; Qiao, Z. W.; Lv, D. F.; Wu, H. X.; Shi, R. F.; Xia, Q. B.; Wang, H. H.; Zhou, J.; Li, Z. Selective adsorption of light alkanes on a highly robust indium based metal-organic framework. *Ind. Eng. Chem. Res.* **2017**, *56*, 4488–4495.

[11] Chen, J. J. In-depth Report on Propylene Industry: Downstream Domestic Substitution Accelerates, Propylene Profits May Increase [Online]. Northeast Securities Co., Ltd., 2021; pp 31–32. https://www.vzkoo.com/read/92d998da7fa309e2d6020c667c9de79e.html.

[12] Geng, D. T.; Zhang, M.; Hang, X. X.; Xie, W. J.; Qin, Y. C.; Li, Q.; Bi, Y. F.; Zheng, Z. P. A 2D metal-thiacalix[4]arene porous coordination polymer with 1D channels: Gas absorption/separation and frequency response. *Dalton Trans.* **2018**, *47*, 9008–9013.

[13] Li, J. R.; Kuppler, R. J.; Zhou, H. C. Selective gas adsorption and separation in metal-organic frameworks. *Chem. Soc. Rev.* **2009**, *38*, 1477–1504.

[14] Wu, T. Y.; Shu, C. J.; Liu, S.; Xu, B. S.; Zhong, S. L.; Zhou, R. F. Separation performance of Si-CHA zeolite membrane for a binary H_2/CH_4 mixture and ternary and quaternary mixtures containing impurities. *Energy Fuels* **2020**, *34*, 11650–11659.

[15] Lin, J. Y. S. Molecular sieves for gas separation. *Science* **2016**, *353*, 121–122.

[16] Shi, R. F.; Lv, D. F.; Chen, Y. W.; Wu, H. X.; Liu, B. Y.; Xia, Q. B.; Li, Z. Highly selective adsorption separation of light hydrocarbons with a porphyrinic zirconium metal-organic framework PCN-224. *Sep. Purif. Technol.* **2018**, *207*, 262–268.

[17] Wang, Y.; Huang, N. Y.; Zhang, X. W.; He, H.; Huang, R. K.; Ye, Z. M.; Li, Y.; Zhou, D. D.; Liao, P. Q.; Chen, X. M. et al. Selective aerobic oxidation of a metal-organic framework boosts thermodynamic and kinetic propylene/propane selectivity. *Angew. Chem., Int. Ed.* **2019**, *131*, 7774–7778.

[18] Cadiau, A.; Adil, K.; Bhatt, P. M.; Belmabkhout, Y.; Eddaoudi, M. A metal-organic framework-based splitter for separating propylene from propane. *Science* **2016**, *353*, 137–140.

[19] Zeng, H.; Xie, M.; Wang, T.; Wei, R. J.; Xie, X. J.; Zhao, Y. F.; Lu, W. G.; Li, D. Orthogonal-array dynamic molecular sieving of propylene/propane mixtures. *Nature* **2021**, *595*, 542–548.

[20] Zhou, D. D.; Chen, P.; Wang, C.; Wang, S. S.; Du, Y. F.; Yan, H.; Ye, Z. M.; He, C. T.; Huang, R. K.; Mo, Z. W. et al. Intermediate-sized molecular sieving of styrene from larger and smaller analogues. *Nat. Mater.* **2019**, *18*, 994–998.

[21] Furukawa, S.; Reboul, J.; Diring, S.; Sumida, K.; Kitagawa, S. Structuring of metal-organic frameworks at the mesoscopic/macroscopic scale. *Chem. Soc. Rev.* **2014**, *43*, 5700–5734.

[22] Adil, K.; Belmabkhout, Y.; Pillai, R. S.; Cadiau, A.; Bhatt, P. M.; Assen, A. H.; Maurin, G.; Eddaoudi, M. Gas/vapour separation using ultra-microporous metal-organic frameworks: Insights into the structure/separation relationship. *Chem. Soc. Rev.* **2017**, *46*, 3402–3430.

[23] Duan, J. G.; Pan, Y. C.; Liu, G. P.; Jin, W. Q. Metal-organic framework adsorbents and membranes for separation applications. *Curr. Opin. Chem. Eng.* **2018**, *20*, 122–131.

[24] Ying, Y. P.; Zhang, Z. Q.; Peh, S. B.; Karmakar, A.; Cheng, Y. D.; Zhang, J.; Xi, L. F.; Boothroyd, C.; Lam, Y. M.; Zhong, C. L. et al. Pressure-responsive two-dimensional metal-organic framework composite membranes for CO_2 separation. *Angew. Chem., Int. Ed.* **2021**, *60*, 11318–11325.

[25] Wang, Y. T.; Hao, C. L.; Fan, W. D.; Fu, M. Y.; Wang, X. K.; Wang, Z. K.; Zhu, L.; Li, Y.; Lu, X. Q.; Dai, F. N. et al. One-step ethylene purification from an acetylene/ethylene/ethane ternary mixture by cyclopentadiene cobalt-functionalized metal-organic frameworks. *Angew. Chem., Int. Ed.* **2021**, *60*, 11350–11358.

[26] Lin, R. B.; Zhang, Z. J.; Chen, B. L. Achieving high performance metal-organic framework materials through pore engineering. *Acc. Chem. Res.* **2021**, *54*, 3362–3376.

[27] Li, B.; Cui, X. L.; O'Nolan, D.; Wen, H. M.; Jiang, M. D.; Krishna, R.; Wu, H.; Lin, R. B.; Chen, Y. S.; Yuan, D. Q. et al. An ideal molecular sieve for acetylene removal from ethylene with record selectivity and productivity. *Adv. Mater.* **2017**, *29*, 1704210.

[28] Assen, A. H.; Belmabkhout, Y.; Adil, K.; Bhatt, P. M.; Xue, D. X.; Jiang, H.; Eddaoudi, M. Ultra-tuning of the rare-earth fcu-MOF aperture size for selective molecular exclusion of branched paraffins. *Angew. Chem., Int. Ed.* **2015**, *54*, 14353–14358.

[29] Hamon, L.; Llewellyn, P. L.; Devic, T.; Ghoufi, A.; Clet, G.; Guillerm, V.; Pirngruber, G. D.; Maurin, G.; Serre, C.; Driver, G. et al. Co-adsorption and separation of CO_2-CH_4 mixtures in the highly flexible MIL-53(Cr) MOF. *J. Am. Chem. Soc.* **2009**, *131*, 17490–17499.

[30] Lin, R. B.; Li, L. B.; Zhou, H. L.; Wu, H.; He, C. H.; Li, S.; Krishna, R.; Li, J. P.; Zhou, W.; Chen, B. L. Molecular sieving of ethylene from ethane using a rigid metal-organic framework. *Nat. Mater.* **2018**, *17*, 1128–1133.

[31] Liang, B.; Zhang, X.; Xie, Y.; Lin, R. B.; Krishna, R.; Cui, H.; Li, Z. Q.; Shi, Y. S.; Wu, H.; Zhou, W. et al. An ultramicroporous metal-organic framework for high sieving separation of propylene from propane. *J. Am. Chem. Soc.* **2020**, *142*, 17795–17801.

[32] Zhang, Z. Q.; Yang, Q. W.; Cui, X. L.; Yang, L. F.; Bao, Z. B.; Ren, Q. L.; Xing, H. B. Sorting of C_4 olefins with interpenetrated hybrid ultramicroporous materials by combining molecular recognition and size-sieving. *Angew. Chem., Int. Ed.* **2017**, *56*, 16282–16287.

[33] Ding, Q.; Zhang, Z. Q.; Yu, C.; Zhang, P. X.; Wang, J.; Cui, X. L.; He, C. H.; Deng, S. G.; Xing, H. B. Exploiting equilibrium-kinetic synergetic effect for separation of ethylene and ethane in a microporous metal-organic framework. *Sci. Adv.* **2020**, *6*, eaaz4322.

[34] Chen, X. Y.; Plonka, A. M.; Banerjee, D.; Krishna, R.; Schaef, H. T.; Ghose, S.; Thallapally, P. K.; Parise, J. B. Direct observation of Xe and Kr adsorption in a Xe-selective microporous metal-organic framework. *J. Am. Chem. Soc.* **2015**, *137*, 7007–7010.

[35] Gan, L.; Chidambaram, A.; Fonquernie, P. G.; Light, M. E.; Choquesillo-Lazarte, D.; Huang, H. L.; Solano, E.; Fraile, J.; Vinas, C.; Teixidor, F. et al. A Highly water-stable *meta*-carborane-based copper metal-organic framework for efficient high-temperature butanol separation. *J. Am. Chem. Soc.* **2020**, *142*, 8299–8311.

[36] Li, L. Y.; Guo, L. D.; Zhang, Z. G.; Yang, Q. W.; Yang, Y. W.; Bao, Z. B.; Ren, Q. L.; Li, J. A robust squarate-based metal-organic framework demonstrates record-high affinity and selectivity for xenon over krypton. *J. Am. Chem. Soc.* **2019**, *141*, 9358–9364.

[37] Andreo, J.; Priola, E.; Alberto, G.; Benzi, P.; Marabello, D.; Proserpio, D. M.; Lamberti, C.; Diana, E. Autoluminescent metal-organic frameworks (MOFs): Self-photoemission of a highly stable thorium MOF. *J. Am. Chem. Soc.* **2018**, *140*, 14144–14149.

[38] Xu, H.; Cao, C. S.; Hu, H. S.; Wang, S. B.; Liu, J. C.; Cheng, P.; Kaltsoyannis, N.; Li, J.; Zhao, B. High uptake of ReO_4^- and CO_2 conversion by a radiation-resistant thorium-nickle $[Th_{48}Ni_6]$ nanocage-based metal-organic framework. *Angew. Chem., Int. Ed.* **2019**, *58*, 6022–6027.

[39] Roztocki, K.; Formalik, F.; Krawczuk, A.; Senkovska, I.; Kuchta, B.; Kaskel, S.; Matoga, D. Collective breathing in an eightfold interpenetrated metal-organic framework: From mechanistic understanding towards threshold sensing architectures. *Angew. Chem., Int. Ed.* **2020**, *59*, 4491–4497.

[40] Yang, H. J.; Trieu, T. X.; Zhao, X.; Wang, Y. X.; Wang, Y.; Feng, P. Y.; Bu, X. H. Lock-and-key and shape-memory effects in an unconventional synthetic path to magnesium metal-organic frameworks. *Angew. Chem., Int. Ed.* **2019**, *58*, 11757–11762.

[41] Taylor, M. K.; Runčevski, T.; Oktawiec, J.; Gonzalez, M. I.; Siegelman, R. L.; Mason, J. A.; Ye, J. X.; Brown, C. M.; Long, J. R. Tuning the adsorption-induced phase change in the flexible metal-organic framework Co(bdp). *J. Am. Chem. Soc.* **2016**, *138*, 15019–15026.

[42] Luo, F.; Yan, C. S.; Dang, L. L.; Krishna, R.; Zhou, W.; Wu, H.; Dong, X. L.; Han, Y.; Hu, T. L.; O'Keeffe, M. et al. UTSA-74: A MOF-74 isomer with two accessible binding sites per metal center for highly selective gas separation. *J. Am. Chem. Soc.* **2016**, *138*, 5678–5684.

[43] Zhang, H. P.; Fan, Y. L.; Krishna, R.; Feng, X. F.; Wang, L.; Luo, F. Robust metal-organic framework with multiple traps for trace Xe/Kr separation. *Sci. Bull.* **2021**, *66*, 1073–1079.

[44] Wang, L.; Yang, L. X.; Gong, L. L.; Krishna, R.; Gao, Z.; Tao, Y.; Yin, W. H.; Xu, Z. Z.; Luo, F. Constructing redox-active microporous hydrogen-bonded organic framework by imide-functionalization: Photochromism, electrochromism, and selective adsorption of C_2H_2 over CO_2. *Chem. Eng. J.* **2020**, *383*, 123117.

[45] Cavka, J. H.; Jakobsen, S.; Olsbye, U.; Guillou, N.; Lamberti, C.; Bordiga, S.; Lillerud, K. P. A new zirconium inorganic building brick forming metal organic frameworks with exceptional stability. *J. Am. Chem. Soc.* **2008**, *130*, 13850–13851.

Electronic Supplementary Material

Th-MOF showing six-fold imide-sealed pockets for middle-size-separation of propane from natural gas

Li Wang[1], Wenhui Zhang[1], Jie Ding[1], Lele Gong[1], Rajamani Krishna[2], Youyuan Ran[1], Lan Chen[1], and Feng Luo[1] (✉)

[1] *Jiangxi Province Key Laboratory of Synthetic Chemistry, School of Chemistry, Biology and Material Science, East China University of Technology, Nanchang 330013, China*
[2] *Van't Hoff Institute for Molecular Sciences, University of Amsterdam, Science Park 904, 1098 XH Amsterdam, The Netherlands*

Supporting information to https://doi.org/10.1007/s12274-022-4915-0

Address correspondence to ecitluofeng@163.com

1. Experimmental section

Synthesis of ECUT-Th-10a: The as-synthesized **ECUT-Th-10** was exchanged with methanol three times every day. After 3-day exchange, the products were evacuated at 100 °C under dynamic vacuum to obtain **ECUT-Th-10a** for confirming the porosity.

Synthesis of UiO-66: $ZrCl_4$ (0.227 mmol, 0.053 g) and 4-Aminobenzoic acid (0.227 mmol, 0.034 g) were dissolved in N,N'-dimethylformamide (DMF, 3 mL) at room temperature. Then the mixture was placed into autoclave and transferred to muffle furnace. The autoclave was heated at 120°C for 24 h. After that, the system was cooled down to room temperature. The obtained UiO-66 were washed by DMF and dried for further use.

Synthesis of activated UiO-66: The as-synthesized UiO-66 was exchanged with methanol three times every day. After 3-day exchange, the products were evacuated at 60°C under dynamic vacuum to obtain activated UiO-66.

X-ray Crystallography

X-ray diffraction data of **ECUT-Th-10** was collected at 298 K on a Bruker-Appex (II) diffractometer using graphite monochromated MoKα radiation (λ=0.71073 Å). The data reduction included a correction for Lorentz and polarization effects, with an applied multi-scan absorption correction (SADABS). The crystal structure was solved and refined using the SHELXTL program suite. Direct methods yielded all non-hydrogen atoms, which were refined with anisotropic thermal parameters. All hydrogen atom positions were calculated geometrically and were riding on their respective atoms. CCDC 2103477 contains the supplementary crystallographic data of **ECUT-Th-10**. The data can be obtained free of charge from the Cambridge Crystallographic Data Centre via www.ccdc.cam.ac.uk/data_request/cif.

Gas adsorption experiments.

The gas sorption isotherms were collected on a Belsorp-max. Roughly 100 mg of **ECUT-Th-10** were taken for the nitrogen adsorption experiments at 77 K. The adsorption isotherms for CH_4, C_2H_6, C_3H_8, and n-C_4H_{10} were obtained at temperature of 273 K and 298 K, respectively. In addition, the adsorption experiments for C_4H_{10} were also performed in 280 K and 290 K. Liquid nitrogen and water bath were used to maintain the experimental temperatures of 77 K, 273 K, and 298 K. Roughly 100 mg of activated UiO-66 were also taken for the single-component adsorption isotherms. The adsorption isotherms for different alkane were measured at 298 K.

Other Instrumentation:

The powder X-ray diffraction (PXRD) patterns were recorded on Bruker AXSD8 Discover powder diffractometer at 40 kV, 40 mA for Cu Kα, (λ= 1.5406 Å) at room temperature. Thermal gravimetric analysis (TGA) was performed using a TGA Q500 thermal analysis system from room temperature to 800 °C under N_2 condition at a constant rate of 10 °C/min.

Calculation of Isosteric Heat of Adsorption

The unary isotherm data for CH_4, C_2H_6, C_3H_8, and n-C_4H_{10} in **ECUT-Th-10a** at 273 K and 298 K were fitted with with the dual-site Langmuir-Freundlich model

$$q = q_{A,sat}\frac{b_A p^{v_A}}{1+b_A p^{v_A}} + q_{B,sat}\frac{b_B p^{v_B}}{1+b_B p^{v_B}} \quad (1)$$

The isosteric heats of adsorption were calculated from the dual-site Langmuir-Freundlich isotherms for **ECUT-Th-10a** using

$$Q_{st} = RT^2\left(\frac{\partial \ln p}{\partial T}\right)_q \quad (2)$$

Where p is the pressure, T is the temperature, R is the gas constant (8.314 J mol^{-1} K^{-1}). By drawing the ln$P$ vs 1/T plot of gas at various loading, Q_{st} = -slope×R.

The obtained parameter and figure were listed as follows.

Table S1 The parameters for Q_{st} calculation for **ECUT-Th-10**

	CH_4	C_2H_6	C_3H_8
a_0	-3210.26781	-3283.68205	-4063.74446
a_1	445.61884	1.00994	290.75002
a_2	-61.96387	-0.57674	-120.24012
a_3	0.42231	0.095374	17.89921
a_4	0.1146	-0.0000274	0.13205
a_5	-0.01061	-0.0000000637	-0.1655
b_0	15.96694	18.78962	17.19628
b_1	-1.79773	-0.21069	-0.09449
b_2	0.18093	0.00159	0.000616
T_1	298	298	298
T_2	273	273	273
R^2	0.99848	0.99805	0.99941

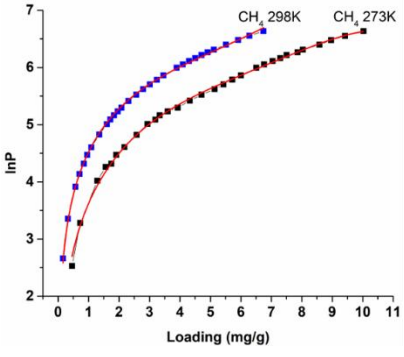

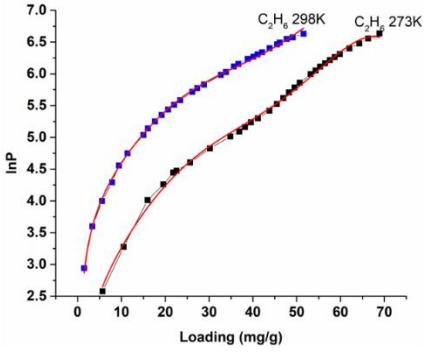

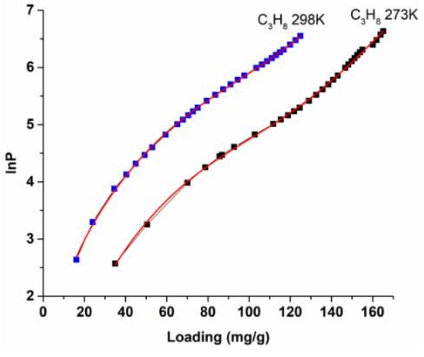

Calculation of selectivity via ideal adsorption solution theory (IAST)

The adsorption selectivity of C_3H_8/CH_4 (50/50), C_3H_8/C_2H_6 (50/50), and C_3H_8/C_4H_{10} (50/50) in **ECUT-Th-10a** and UiO-66 was established by the Ideal Adsorbed Solution Theory (IAST). The adsorption selectivity was calculated from

$$S_{ads} = \frac{q_A/q_B}{y_A/y_B} \quad (2)$$

where the q_A, and q_B represent the molar loadings in **ECUT-Th-10a** or UiO-66 that is in equilibrium with a bulk fluid mixture with mole fractions y_A, and $y_B = 1 - y_A$. The molar loadings, also called *gravimetric uptake capacities*, are expressed in mol kg^{-1}.

Table S2. Dual-site Langmuir-Freundlich parameter fits for CH_4, C_2H_6, C_3H_8, and nC_4H_{10} in **ECUT-Th-10** at 298 K.

	Site A			Site B		
	$q_{A,sat}$ mol kg^{-1}	b_A $Pa^{-\nu A}$	ν_A	$q_{B,sat}$ mol kg^{-1}	b_B $Pa^{-\nu B}$	ν_B
CH_4	2.5	9.040E-07	1	0.6	5.185E-06	1
C_2H_6 [a]	3.1	1.002E-05	1			
C_3H_8	3.7	1.679E-05	1	0.62	3.795E-04	1
nC_4H_{10}	2.5	2.30771E-20	4.45	2.2	1.28601E-13	1

a The fit was based on 1-site Langmuir.

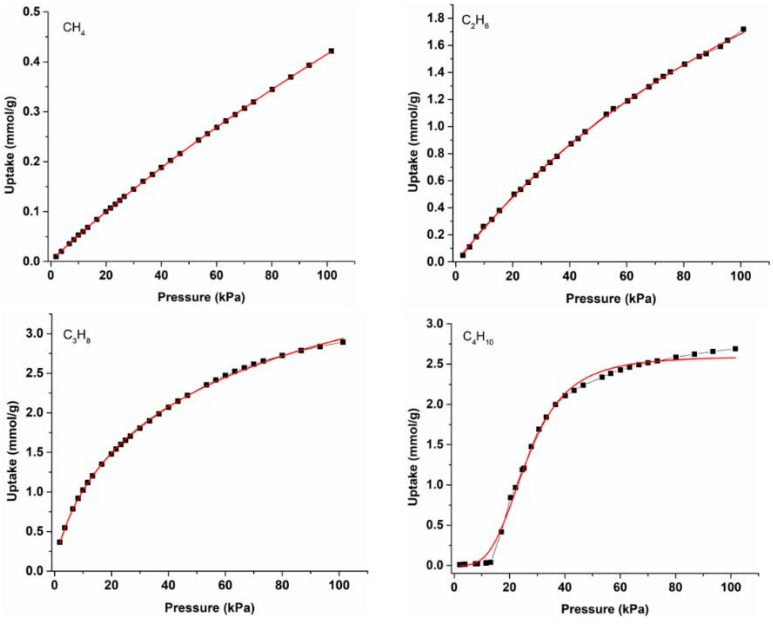

Table S3. 1-site Langmuir parameter fits for CH_4, C_2H_6, C_3H_8, and nC_4H_{10} in UiO-66 at 298 K.

	q_{sat} mol kg^{-1}	b Pa^{-1}
CH_4	10.9	4.575E-07
C_2H_6	3.3	2.576E-05
C_3H_8	5.1	3.156E-05
nC_4H_{10}	5.3	7.411E-05

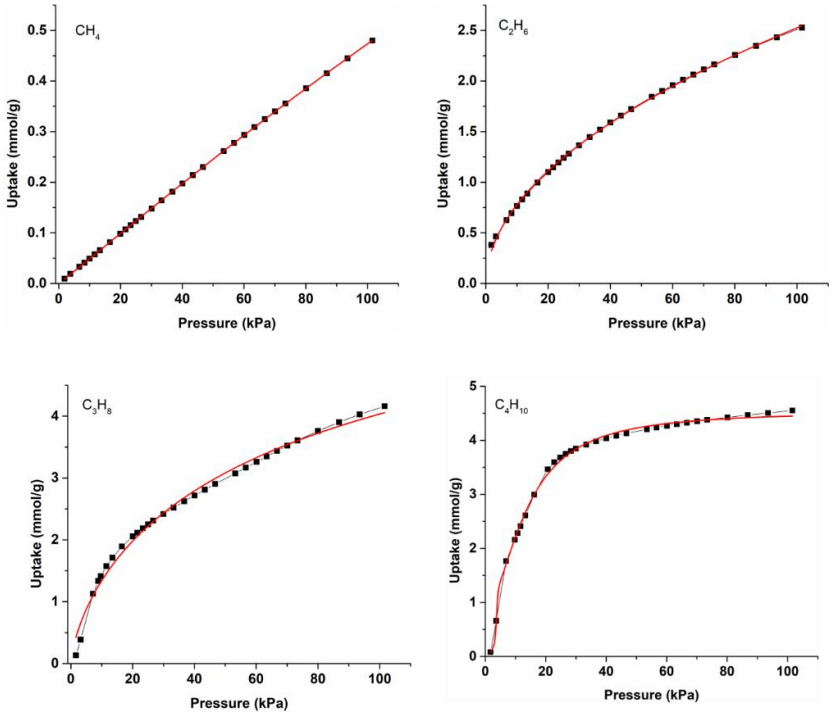

Breakthrough experiments.

The breakthrough experiments were performed at 298 K. Bulk **ECUT-Th-10a** (around 500 mg) were filled into stainless steel column (Φ 46 mm×150 mm). First, the helium gas (100 mL/min) was introduced into the column for 30 min. Then the different gas mixture C_2H_6/C_3H_8 (50/50, v/v), $CH_4/C_2H_6/C_3H_8$ (33/33/33, v/v/v), $C_2H_6/C_3H_8/C_4H_{10}$ (33/33/33, v/v/v), $CH_4/C_2H_6/C_3H_8/C_4H_{10}$ (25/25/25/25, v/v/v/v), and simulated natural gas passed through the column with 2 mL/min for 2-component and 3-component) and 1 mL/min for 4-component and simulated nature gas. The eluted gas stream from the column is monitored by a Hiden mass-spectrometer. Prior to each cycling experiment, the adsorption bed was regenerated by He flow for 3h at 333 K to ensure complete removal of adsorbed gas.

Density Functional Theory Calculations

The density functional theory (DFT) calculations were performed by using the Vienna Ab initio Simulation Package (VASP) code with the projector augmented wave (PAW) method.[1,2] The exchange-functional was treated using the generalized gradient approximation (GGA) of Perdew-Burke-Ernzerhof (PBE) functional.[3] Wave functions were expanded using a plane-wave basis set with kinetic energy cutoff of 400 eV and the geometries were fully relaxed until the residual force convergence value on each atom being less 0.02 eV/Å. The Brillouin zone integration was performed using 2×2×2 Monkhorst-Pack k-point sampling for a primitive cell.[4] The self-consistent calculations applied a convergence energy threshold of 10^{-5} eV. Spin-polarization was considered in all calculations.[5] The vdW interaction was controlled *via* zero damping DFT-D3 method. The above parameters have been optimized until the energy change is negligible.

The single molecular adsorption energy of those alkanes were calculated with following equation[6]:

$$\mathrm{Th-MOF} + nL \rightarrow \mathrm{Th-MOF}(L)$$

$$\Delta G = [\Delta G_{Th-MOF(L)_n} - \Delta G_{Th-MOF} - n \times \Delta G_L]$$

where the L means alkane molecules, such as methane, ethane, propane or butane.

2. Characterization

Table S4. The crystal data and structure refinements for **ECUT-Th-10**

Compound	**ECUT-Th-10**
Formula	$C_{84}H_{36}N_6O_5Th_3$
Formula weight	2273.31
Color	Light orange
Crystal system	cubic
Space group	*Fd-3m*
a(Å)	39.5857(7)
b(Å)	39.5857(7)
c (Å)	39.5857(7)
α	90.00
β	90.00
γ	90.00
Volume (Å^3)	62032(3)
Z	16
Temperature for data collection (K)	296
Range for data collection θ(°)	2 to 25
No. of measured reflections	14203
No. of unique reflections	2599
No. of parameters	116
No. of restraints	94
Goodness-of-fit on F^2	0.969
Final R indexes[I≥2σ(I)]	R_1=0.0673, wR_2=0.1912
Final R indexes [all data]	R_1=0.1180, wR_2=0.2128

[a]$R_1 = \Sigma||F_o|-|F_c||/\Sigma|F_o|$. [b]$wR_2 = [\Sigma w\ (F_o^2-F_c^2)^2/\Sigma w\ (F_o^2)^2]^{1/2}$.

Table S5 Selected bond length (Å) and angles (°) for **ECUT-Th-10**

Bond length

Th(1)-O(2)#5	2.276(3)	Th(1)-O(1)#7	2.461(8)
Th(1)-O(3)#3	2.494(4)	Th(1)-O(1) #8	2.461(8)
Th(1)-O(1)#6	2.461(8)		

Symmetrical code: #1 +X,5/4-Z,5/4-Y; #2 +X,7/4-Y,3/4-Z; #3 -1+Y,5/4-X,1/4-Z; #4 +Z,1+X,-1+Y; #5 5/4-Y,1+X,1/4-Z; #6 1/4-X,+Y,1/4-Z; #7 +Z,+Y,+X; #8 1/4-Z,+Y,1/4-X

Bond angles

O(2)-Th(1)-O(2)#5	89.1(8)	O(1)#8- Th (1)-O(1)#7	126.4(5)
O(2)#5-Th(1)-O(3)#3	69.8(3)	O(1)#8- Th (1)-O(3)#3	72.0(4)
O(2)#5-Th(1)-O(3)	69.8(3)	O(1)- Th (1)-O(3)	138.2(3)
O(2)-Th(1)-O(3)#3	69.8(3)	O(1)#8- Th (1)-O(3)	138.2(3)
O(2)-Th(1)-O(3)	69.8(3)	O(1)#6- Th (1)-O(3)	72.0(4)
O(2)-Th(1)-O(1)#6	81.9(4)	O(1)- Th (1)-O(3)#3	72.0(4)
O(2)-Th(1)-O(1)	141.5(3)	O(1)#7- Th (1)-O(3)	72.0(4)
O(2)-Th(1)-O(1)#7	141.5(3)	O(1)#6- Th (1)-O(3)#3	138.2(3)
O(2)#5-Th(1)-O(1)#8	141.5(3)	O(1)#7- Th (1)-O(3)#3	138.2(3)
O(2)#5-Th(1)-O(1)	81.9(4)	O(1)#8- Th (1)-O(1)#6	74.2(5)
O(2)#5-Th(1)-O(1)#6	141.5(3)	O(1)#6- Th (1)-O(1)#7	82.3(6)
O(2)-Th(1)-O(1)#8	81.9(4)	O(1)#8- Th (1)-O(1)	82.3(6)
O(2)#5-Th(1)-O(1)#7	81.9(4)	O(1)#6- Th (1)-O(1)	126.4(5)
O(3)#3-Th(1)-O(3)	122.1(8)	O(1)- Th (1)-O(1)#7	74.2(5)

Symmetrical code: #1 +X,5/4-Z,5/4-Y; #2 +X,7/4-Y,3/4-Z; #3 -1+Y,5/4-X,1/4-Z; #4 +Z,1+X,-1+Y; #5 5/4-Y,1+X,1/4-Z; #6 1/4-X,+Y,1/4-Z; #7 +Z,+Y,+X; #8 1/4-Z,+Y,1/4-X

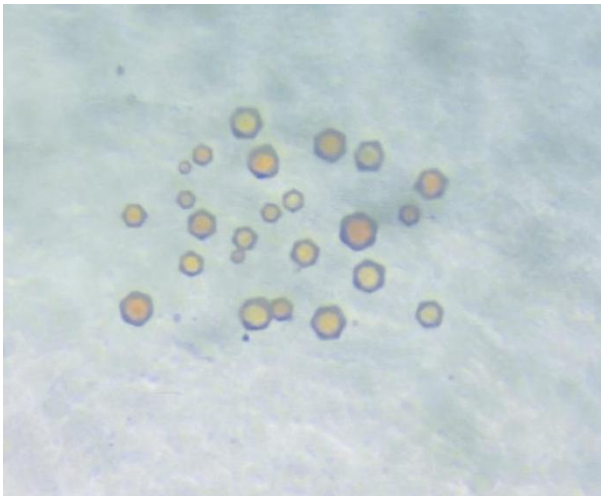

Fig. S1 The optical microscope image of **ECUT-Th-10.**

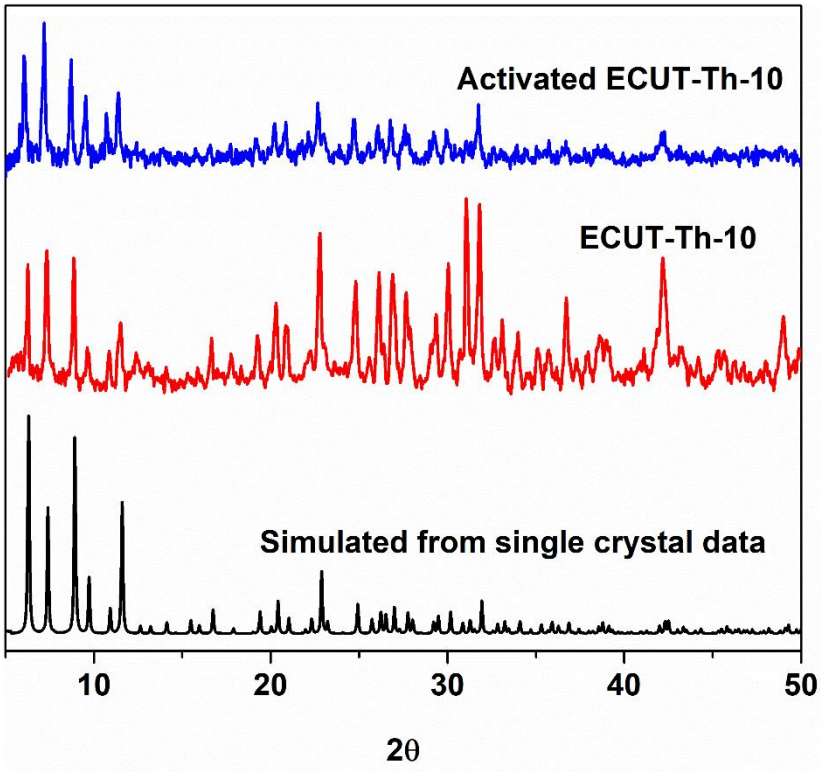

Fig. S2 Powder X-ray diffraction pattern of **ECUT-Th-10** and simulated pattern from single crystal data.

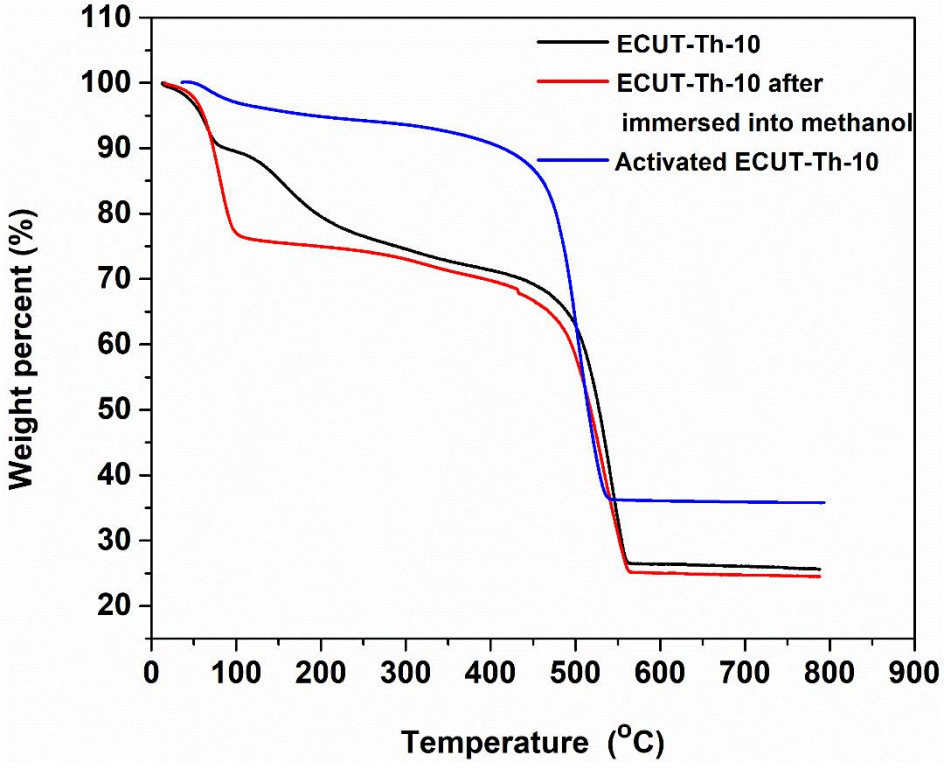

Fig. S3 Thermal analysis of **ECUT-Th-10** from room temperature to 800℃.

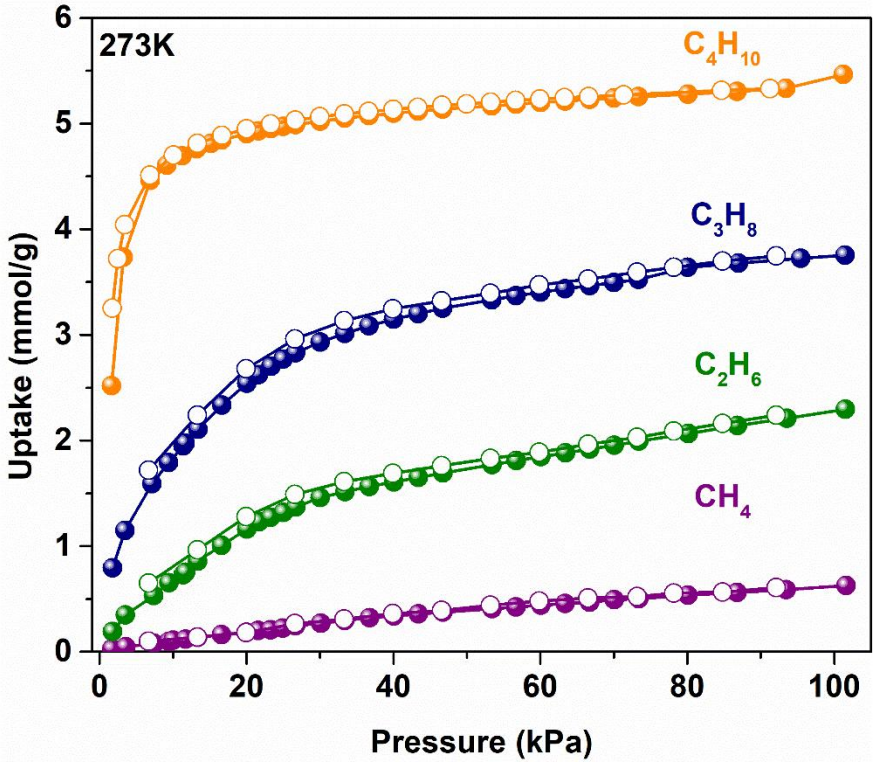

Fig. S4 The adsorption isotherms of **ECUT-Th-10** for CH_4, C_2H_6, C_3H_8 and C_4H_{10} at 273 K, respectively.

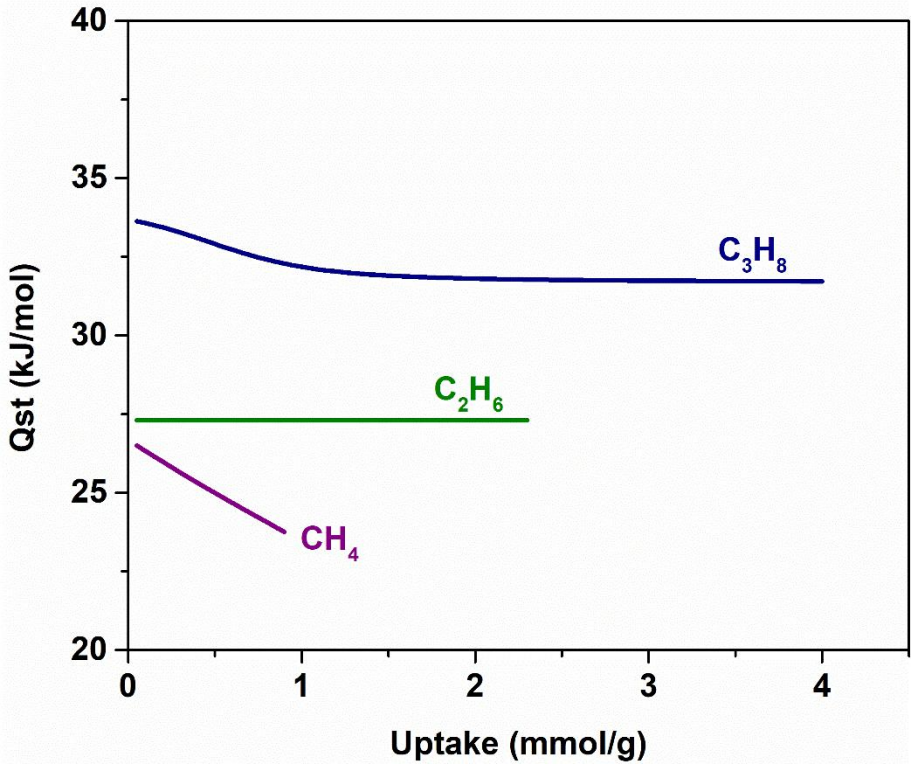

Fig. S5 The isosteric heat of adsorption for CH_4, C_2H_6 and C_3H_8 in **ECUT-Th-10**.

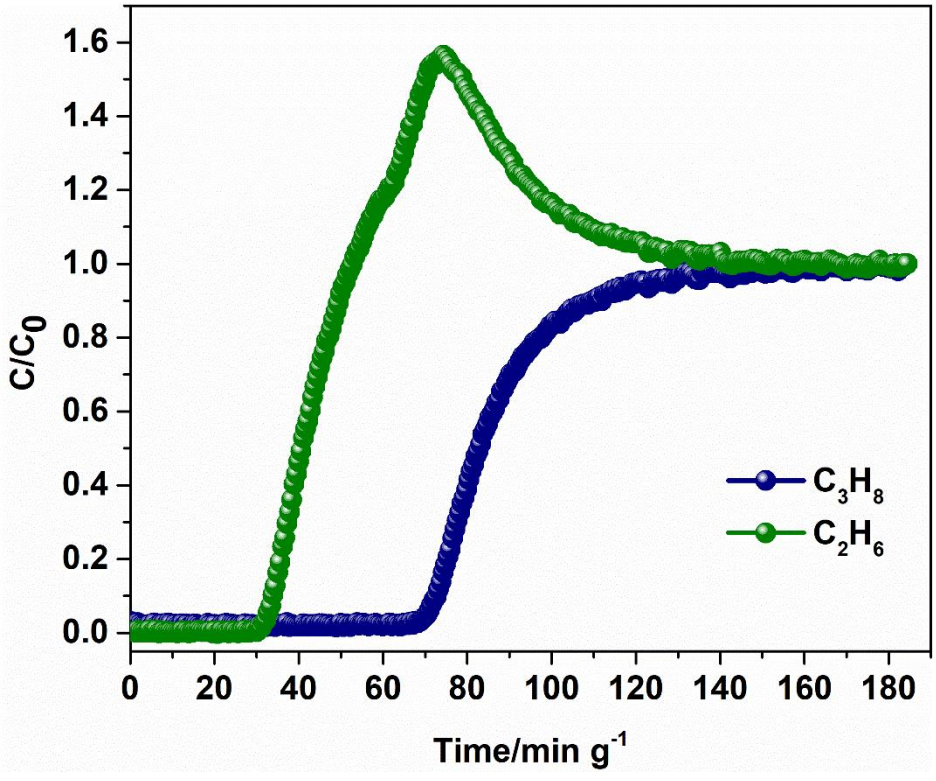

Fig. S6 Experimental breakthrough curves of **ECUT-Th-10** for C_2H_6/C_3H_8 (50/50, v/v) binary mixture at 298 K.

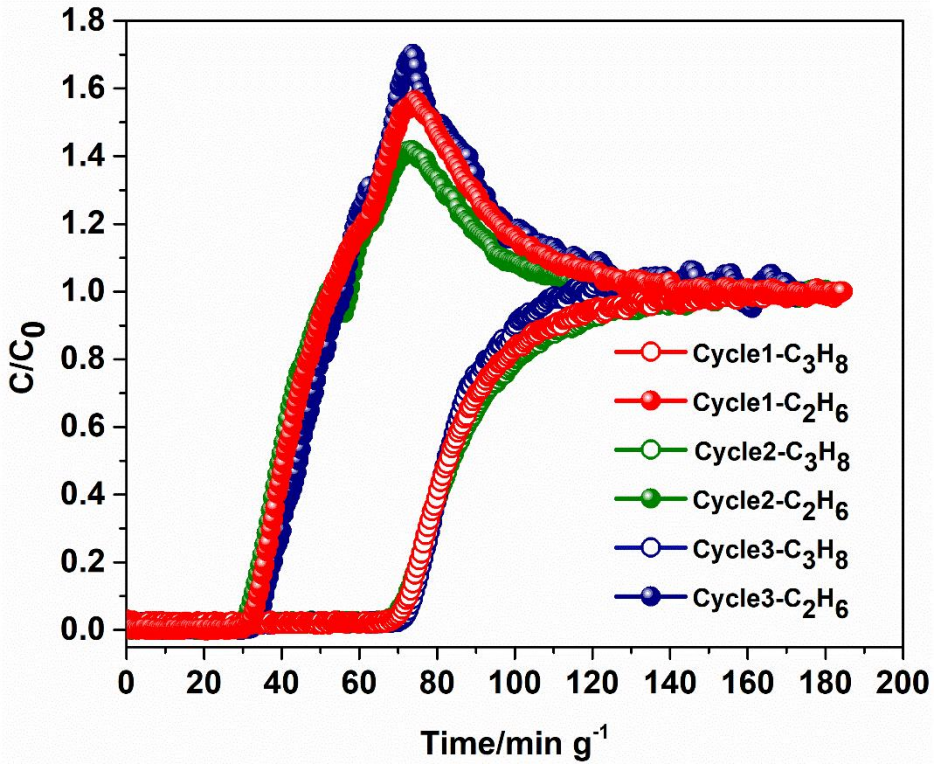

Fig. S7 Experimental breakthrough curves at 298 K on **ECUT-Th-10** with C_2H_6/C_3H_8 (50/50, v/v) binary mixture for three cycles.

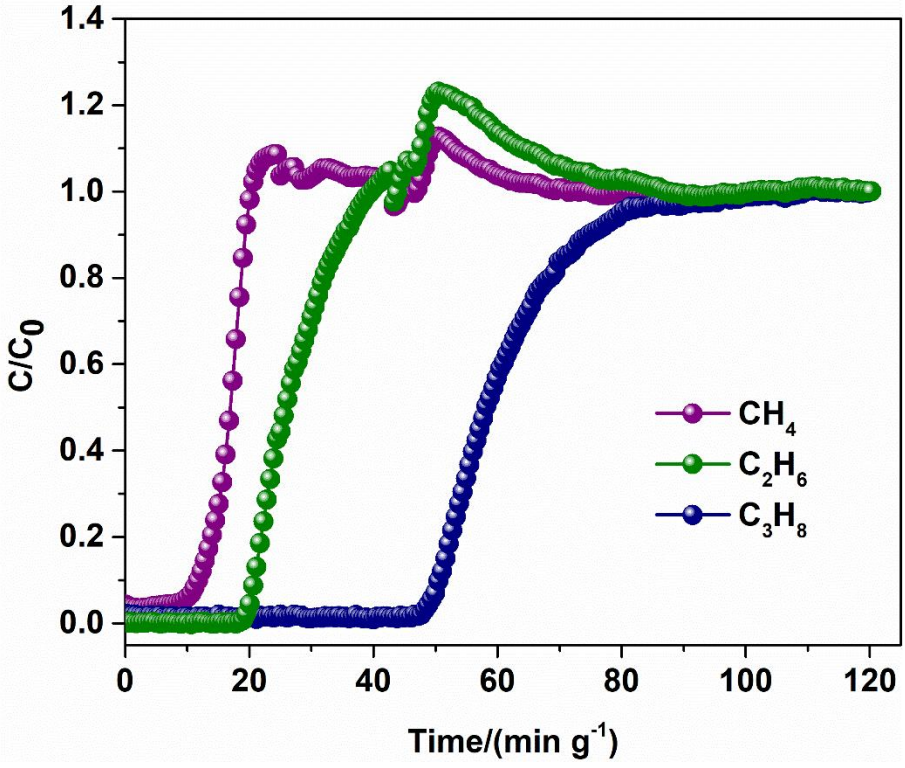

Fig. S8 Experimental breakthrough curves of **ECUT-Th-10** for $CH_4/C_2H_6/C_3H_8$ (33/33/33, v/v/v) 3-component mixture at 298 K.

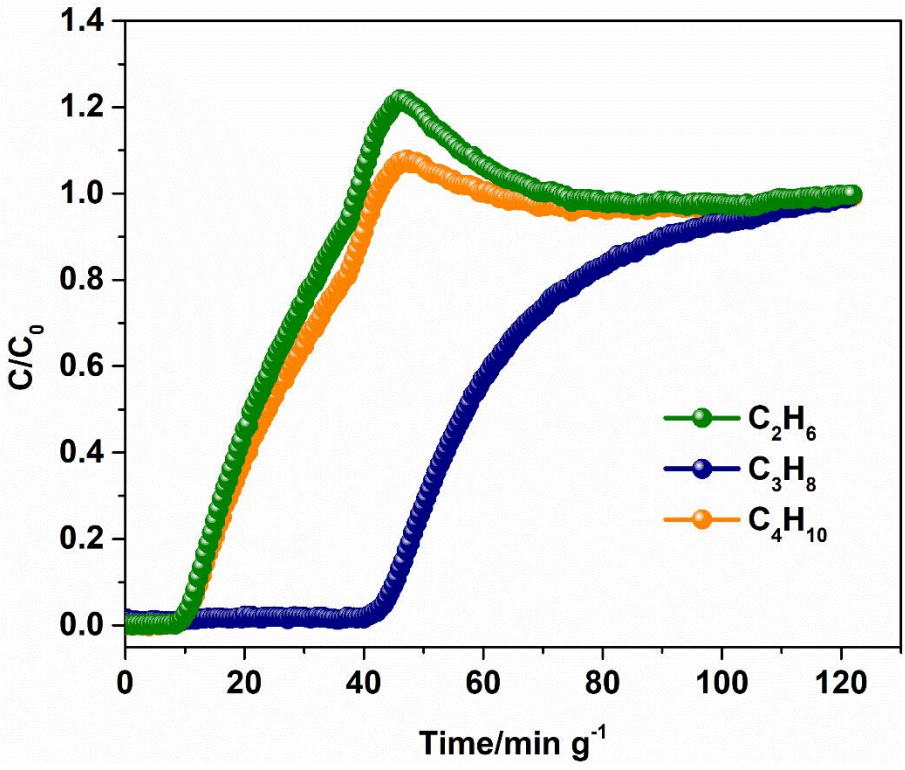

Fig. S9 Experimental breakthrough curves of **ECUT-Th-10** for $C_2H_6/C_3H_8/C_4H_{10}$ (33/33/33, v/v/v) 3-component mixture at 298 K.

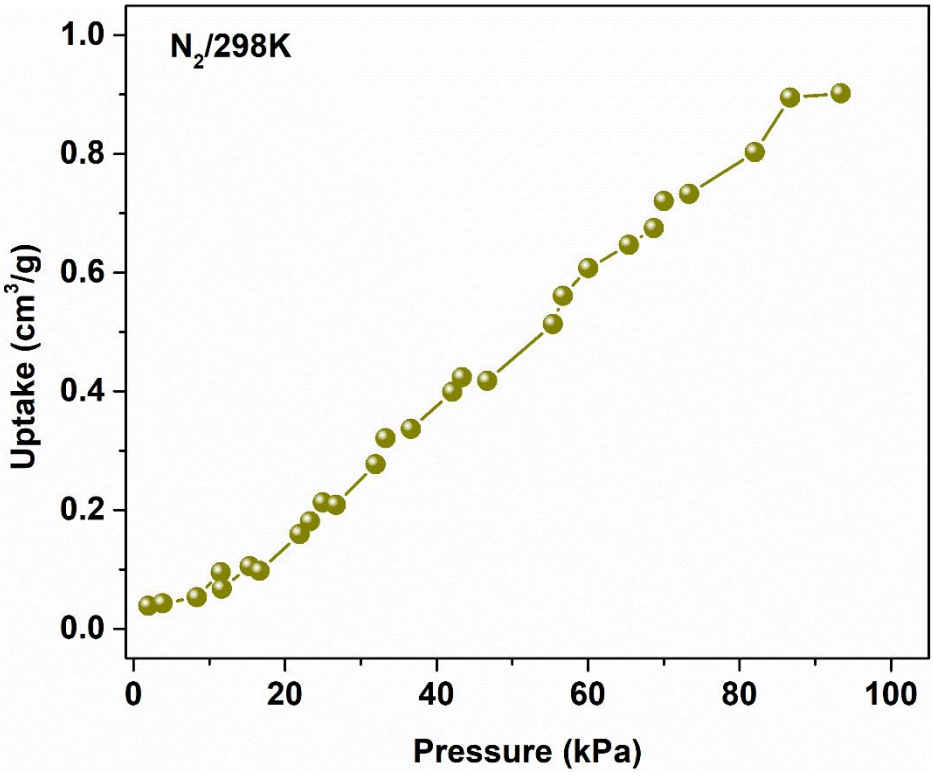

Fig. S10 The adsorption isotherm of **ECUT-Th-10** for N_2 at 298 K.

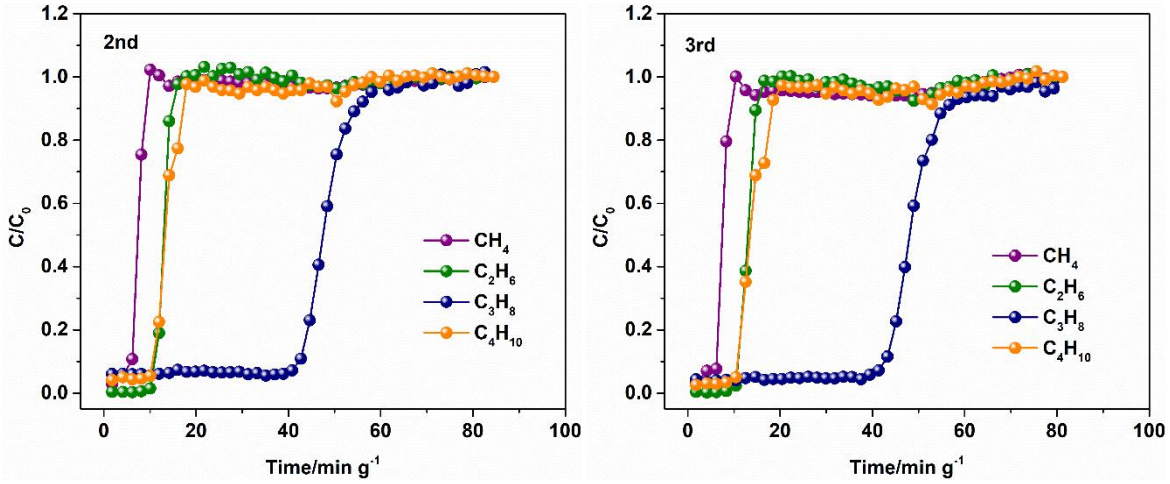

Fig. S11 Experimental breakthrough curves at 298 K on **ECUT-Th-10** with simulated natural gas for another two times.

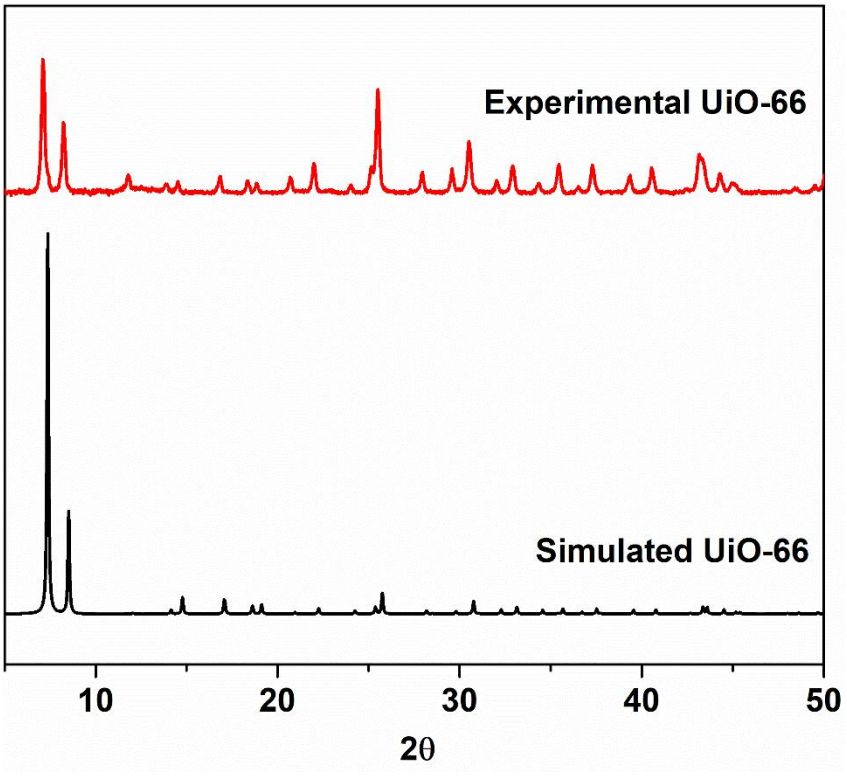

Fig. S12 Powder X-ray diffraction pattern of synthesized UiO-66 in this work and simulated UiO-66.

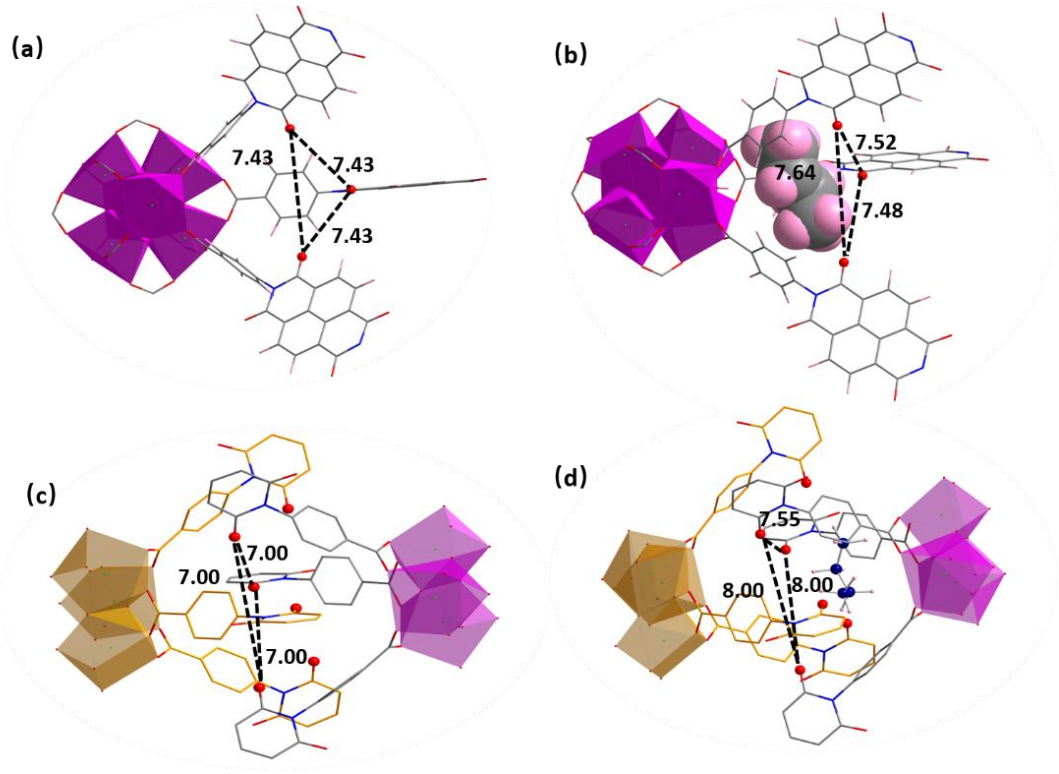

Fig. S13 The three-fold imide-sealed pockets without C_4H_{10} (a) and with C_4H_{10} (b). The three-fold imide-sealed pockets without C_4H_{10} (c) and with C_4H_{10} (d). The adsorption of C_4H_{10} in the three-fold imide-sealed pockets does not cause structure change since the O···O distance between the three imide ligands remained more or less identical. However, this distance was enlarged almost 1 Å to accommodate C_4H_{10} in six-fold imide-sealed pockets, leading to the obvious distortion of the structure.

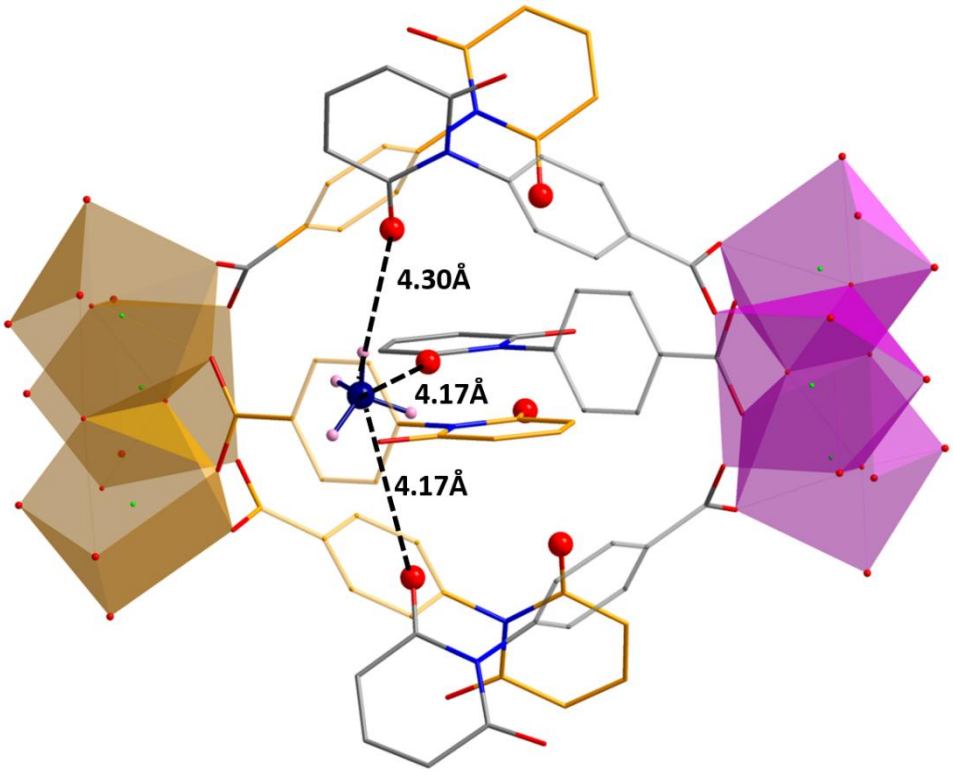

Fig. S14 The calculated (C)H($^{\delta+}$) ···($^{\delta-}$)O(C) interactions between CH_4 and imide units in **ECUT-Th-10**.

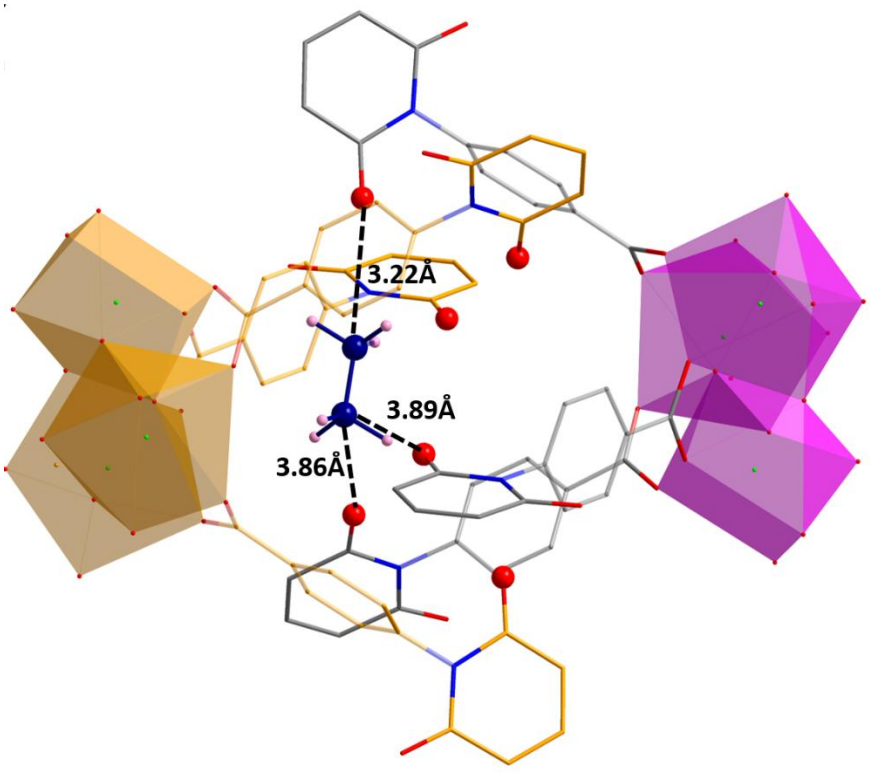

Fig. S15 The calculated (C)H($^{\delta+}$) ···($^{\delta-}$)O(C) interactions between C_2H_6 and imides units in **ECUT-Th-10**.

Supplementary References

[1] Perdew, J. P.; Burke, K.; Ernzerhof, M, Generalized Gradient Approximation Made Simple. *Phys. Rev. lett.* **77**, 3865 (1996).

[2] Kresse, G.; Joubert, D. From ultrasoft pseudopotentials to the projector augmented-wave method. *Phys. Rev. B.* **59**, 1758 (1999).

[3] Kim, H.; Lee, K.; Woo, S. I.; Jung, Y. On the mechanism of enhanced oxygen reduction reaction in trogen-doped graphene nanoribbons. *Phys. Chem. Chem. Phys.* **13**, 17505-17510 (2011).

[4] Chadi, D. Special points for Brillouin-zone integrations. *Phys. Rev. B.* **16**, 1746-1747 (1977).

[5] L. Gong, D. Zhang, C.-Y. Lin, Y. Zhu, Y. Shen, J. Zhang, X. Han, L. Zhang, Z. Xia, Catalytic mechanisms and design principles for single-atom catalysts in highly efficient CO_2 conversion. *Adv. Energy Mater.* **9**, 1902625 (2019).

[6] L. Gong, D. Zhang, Y. Shen, X. Wang, J. Zhang, X. Han, L. Zhang, Z. Xia, Enhancing both selectivity and activity of CO_2 conversion by breaking scaling relations with bimetallic active sites anchored in covalent organic frameworks. *J. Catal.* **390**, 126-134 (2020).

Address correspondence to ecitluofeng@163.com